Investigation of the low-temperature AlGaN interlayer in AlGaN/GaN/AlGaN double heterostructure on Si substrate

2014 Appl. Phys. Express 7 115501

(http://iopscience.iop.org/1882-0786/7/11/115501)

Applied Physics Express 7, 115501 (2014)
http://dx.doi.org/10.7567/APEX.7.115501

Investigation of the low-temperature AlGaN interlayer in AlGaN/GaN/AlGaN double heterostructure on Si substrate

Yu-Lin Hsiao[1], Yi-Jie Wang[2], Chia-Ao Chang[1], You-Chen Weng[3], Yen-Yu Chen[1], Kai-Wei Chen[1], Jer-Shen Maa[3], and Edward Yi Chang[1]*

[1]*Department of Materials Science and Engineering, National Chiao Tung University, Hsinchu 30010, Taiwan*
[2]*Institute of Photonic System, College of Photonics, National Chiao Tung University, Tainan 71150, Taiwan*
[3]*Institute of Lighting and Energy Photonics, College of Photonics, National Chiao Tung University, Tainan 71150, Taiwan*
E-mail: edc@mail.nctu.edu.tw

Received August 1, 2014; accepted September 24, 2014; published online October 9, 2014

A low-temperature (LT) AlGaN interlayer is inserted in the $Al_{0.1}Ga_{0.9}N$ back barrier layer of an $Al_{0.2}Ga_{0.8}N/GaN/Al_{0.1}Ga_{0.9}N$ double heterostructure grown on a 150 mm Si substrate. It is found that the 21-nm-thick LT-AlGaN interlayer plays an important role in stress relaxation and dislocation reduction of the $Al_{0.1}Ga_{0.9}N$ back barrier layer, especially for screw dislocation reduction. In addition, a buffer breakdown voltage higher than 600 V is achieved, which is much higher than those of conventional heterostructures. These results demonstrate the effectiveness of combining the LT-AlGaN interlayer and the $Al_{0.2}Ga_{0.8}N/GaN/Al_{0.1}Ga_{0.9}N$ double heterostructure on a Si substrate to increase the breakdown voltage for high-power applications.

In the past decade, AlGaN/GaN single-heterostructure field-effect transistors on Si substrates with high breakdown voltage and low specific on-resistance characteristics were studied extensively.[1–4] Excellent electrical performance characteristics make GaN devices attractive for high-power switching applications. Furthermore, the fabrication cost of GaN grown on large-diameter Si substrates is much lower than those of GaN-on-SiC and GaN-on-sapphire wafers devices. Recently, 600 V GaN-on-Si commercial power devices have become available with price and performance comparable to those of traditional Si-based power devices.[5] It is expected that GaN-on-Si devices will further improve the power efficiency with reduced production cost and become a strong competitor for power electronic markets in the near future.[6,7]

The epitaxial growth of GaN on Si is the most critical step in the fabrication of GaN power devices. Over the last few years, reports on enhancing the breakdown voltage have focused mainly on modifying the epitaxial structure. For example, the crystalline quality of the GaN layer can be improved by growing on a thick epitaxial buffer layer, thereby blocking the passage of leakage current from the high-dislocation-density layer.[8,9] In order to grow this thick GaN layer, the strain engineering design is crucial to compensate for the large lattice and thermal mismatches between GaN and Si. Inserting a thin low-temperature (LT) interlayer (AlN, InN, or AlGaN) into the GaN can induce a compressive stress that can compensate for the large tensile stress generated during the cooling step.[10–12] The effectiveness of this LT interlayer has been demonstrated by several groups to optimize the GaN-on-Si growth.[13–17] A different approach to achieve a high breakdown voltage based on the use of an AlGaN/GaN/AlGaN double heterostructure has been proposed. The electron confinement is more effective and the breakdown field becomes higher after adding the AlGaN back barrier.[18,19] All the previous studies demonstrated the potential advantages of combining the LT-AlGaN interlayer and the AlGaN/GaN/AlGaN double heterostructure on large-diameter Si substrates.

In this work, we propose a novel $Al_{0.2}Ga_{0.8}N/GaN/Al_{0.1}Ga_{0.9}N$ double heterostructure grown on a 150 mm Si substrate with the insertion of a LT-AlGaN interlayer within the $Al_{0.1}Ga_{0.9}N$ back barrier layer. The effects of the LT-AlGaN interlayer on stress relaxation, dislocation density reduction, and increase in the buffer breakdown voltage are presented. A buffer breakdown voltage higher than 600 V is demonstrated.

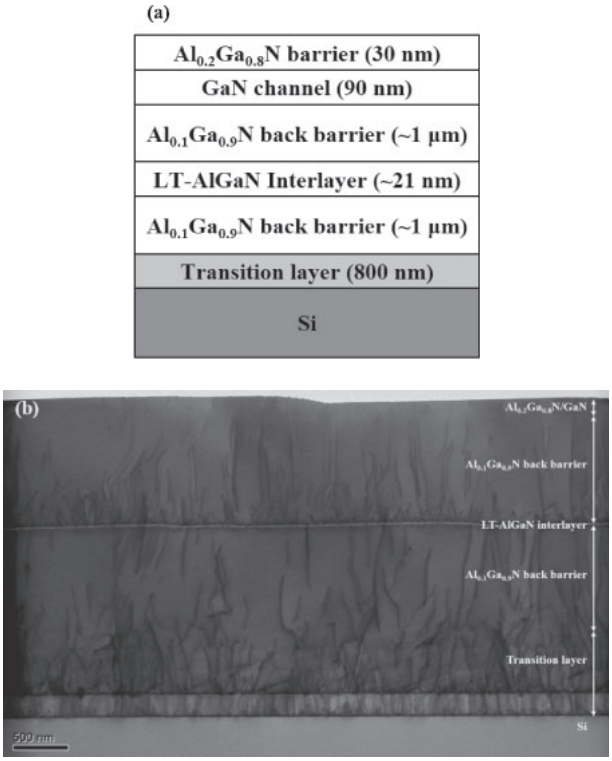

Fig. 1. (a) Schematic diagram of the $Al_{0.2}Ga_{0.8}N/GaN/Al_{0.1}Ga_{0.9}N$ double heterostructure on Si substrate with the inserted LT-AlGaN interlayer and (b) cross-sectional TEM image of the whole epitaxial layer structure.

This proposed structure is shown in Fig. 1(a) and the cross-sectional transmission electron microscopy (TEM) image of the complete epitaxial structure of the $Al_{0.2}Ga_{0.8}N/GaN/Al_{0.1}Ga_{0.9}N$ double heterostructure with the LT-AlGaN interlayer grown on Si is shown in Fig. 1(b). The epitaxial growth of these layers on the 150 mm Si(111) substrate was carried out in a Thomas Swan metalorganic chemical vapor deposition (MOCVD) system. Trimethylaluminum (TMAl), trimethylgallium (TMGa), and ammonia were used as the precursors for Al, Ga, and N, respectively.

H_2 was used as the carrier gas. The growth sequence is as follows: an 800-nm-thick transition layer consisting of AlN and multi-AlGaN layers was first grown on the Si substrate, which was followed by the growth of a 1-μm-thick $Al_{0.1}Ga_{0.9}N$ back barrier layer. In the subsequent growth of the 2-μm-thick $Al_{0.1}Ga_{0.9}N$ back barrier layer, a thin LT-AlGaN interlayer was inserted between two 1-μm-thick $Al_{0.1}Ga_{0.9}N$ back barrier layers. The growth was completed after the growth of a 90-nm-thick GaN channel layer and a 30-nm-thick $Al_{0.2}Ga_{0.8}N$ top barrier layer. For the buffer breakdown voltage comparison, two conventional structures, namely, an $Al_{0.2}Ga_{0.8}N$/GaN single heterostructure with a LT interlayer and an $Al_{0.2}Ga_{0.8}N$/GaN/$Al_{0.1}Ga_{0.9}N$ double heterostructure without a LT interlayer, were grown on the same transition layer. Details of the epitaxial growth of these two control samples can be found in our previous work.[19)]

During the epitaxial growth, the wafer temperature, reflectance, and wafer curvature were in situ-monitored using a Laytec EpiCurve® TT system. The structure and composition of each layer were characterized by secondary ion mass spectrometry (SIMS), high-resolution X-ray diffraction (HRXRD), and weak-beam dark-field TEM.

In order to further confirm the buffer quality of the two conventional structures and the proposed structure, the buffer breakdown voltage characteristics of these samples were measured using Agilent B1505A. The isolation regions were defined by Cl_2-based dry etching. The electrodes of a Ti/Al/Ni/Au multilayer metal were deposited using an electron beam evaporator, followed by rapid thermal annealing at 800 °C for 60 s under N_2 atmosphere. The contact resistances of these samples were in the range of 0.5–0.6 Ω mm based on the transmission line model method. The gate metal of Ni/Au was deposited as a Schottky gate electrode using an electron beam evaporator. An off-state breakdown voltage was measured on the proposed structure sample to prove the real advantages of the fabricated device. The gate width (W_g), gate length (L_g), gate-to-drain spacing (L_{gd}), and gate-to-source spacing (L_{gs}) were 100, 1, 4.5, and 1.5 μm, respectively.

Previously, Fritze et al. investigated the impact of LT-AlGaN interlayer thickness on the stress and crystalline quality of the GaN-on-Si structure.[12)] It was found that the role of the LT-AlGaN interlayer was to introduce additional compressive stress to compensate for the tensile stress generated in the thick epilayers. On the basis of this concept, it is expected that a similar benefit will be obtained by adding a LT-AlGaN interlayer into the thick $Al_{0.1}Ga_{0.9}N$ back barrier layer of the $Al_{0.2}Ga_{0.8}N$/GaN/$Al_{0.1}Ga_{0.9}N$ double heterostructure.

The stress evolution during the $Al_{0.1}Ga_{0.9}N$ back barrier layer growth can be observed from the in situ wafer curvature measurement. Figure 2 shows the results of the in situ measurements of temperature, reflectance, and wafer curvature obtained with a Laytec EpiCurve® TT system during the growth of the $Al_{0.2}Ga_{0.8}N$/GaN/$Al_{0.1}Ga_{0.9}N$ double heterostructure. The first $Al_{0.1}Ga_{0.9}N$ back barrier layer was grown under a compressive stress (negative curvature). It was attributed to the larger in-plane lattice constant of $Al_{0.1}Ga_{0.9}N$ than of the transition layer. However, if the first $Al_{0.1}Ga_{0.9}N$ back barrier layer is thicker than 1 μm, this compressive stress will be relaxed with dislocation formation and converted to tensile stress. A LT-AlGaN interlayer was inserted in the middle of the 2-μm-thick $Al_{0.1}Ga_{0.9}N$ back barrier layer

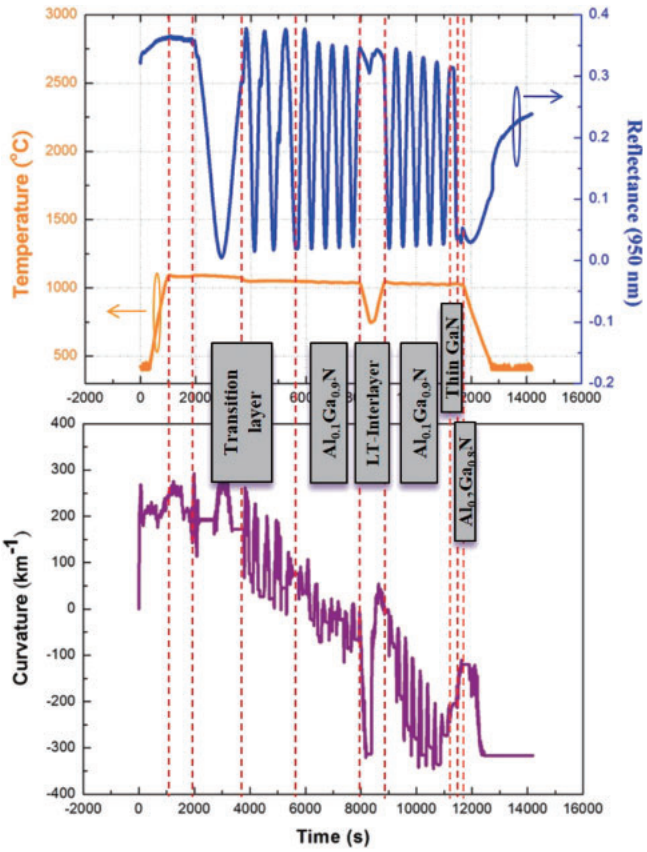

Fig. 2. In situ measurements of temperature, reflectance, and wafer curvature during the growth of AlGaN/GaN/AlGaN double heterostructure.

in order to prevent this stress transition. The inserted LT-AlGaN interlayer was grown at 750 °C for 180 s. A negative curvature trace was observed during the growth of the $Al_{0.1}Ga_{0.9}N$ back barrier layer with the insertion of the LT-AlGaN interlayer, which indicates that an effective compressive stress was induced by this LT-AlGaN interlayer.

In order to investigate the details of each epilayer, the SIMS depth profiles of Al and Ga on the $Al_{0.2}Ga_{0.8}N$/GaN/$Al_{0.1}Ga_{0.9}N$ double heterostructure were analyzed, and the results are shown in Fig. 3. From the depth profiles, increases in the intensities of Al- and Ga-related signals were observed near 1125 nm below the surface. This provides evidence of the existence of the AlGaN interlayer between the two $Al_{0.1}Ga_{0.9}N$ back barrier layers. From the inset of Fig. 3, a 21-nm-thick LT-AlGaN interlayer can be clearly observed from the TEM image. However, the Al signal is only for qualitative analysis, not for quantitative analysis; further investigation is needed to characterize the Al composition of the LT-AlGaN interlayer.

The Al composition is estimated to be 50% for the LT-AlGaN interlayer as judged from the HRXRD ω–2θ scan data shown in Fig. 4. Owing to the thin interlayer, the intensity of the $Al_{0.5}Ga_{0.5}N$(002) peak is low. On the other hand, the $Al_{0.1}Ga_{0.9}N$ back barrier layer shows a very high peak intensity. The $Al_{0.1}Ga_{0.9}N$ layer provides a higher conduction band discontinuity that helps prevent the electron leakage from the channel layer. Furthermore, according to the XRD rocking curve, the full-widths at half-maximum (FWHMs) of X-ray rocking curves for the $Al_{0.1}Ga_{0.9}N$(002) ω-scan and $Al_{0.1}Ga_{0.9}N$(102) ω-scan were 578.6 and 1103 arcsec, re-

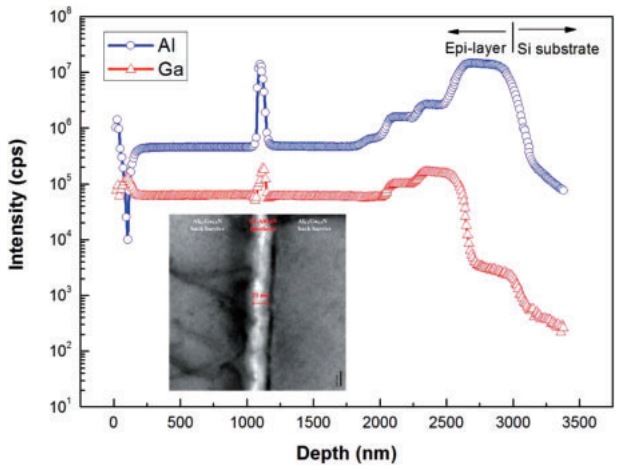

Fig. 3. SIMS depth profiles of Al and Ga for the proposed structure. The inset shows the interface between the LT-AlGaN interlayer and two AlGaN back barrier layers.

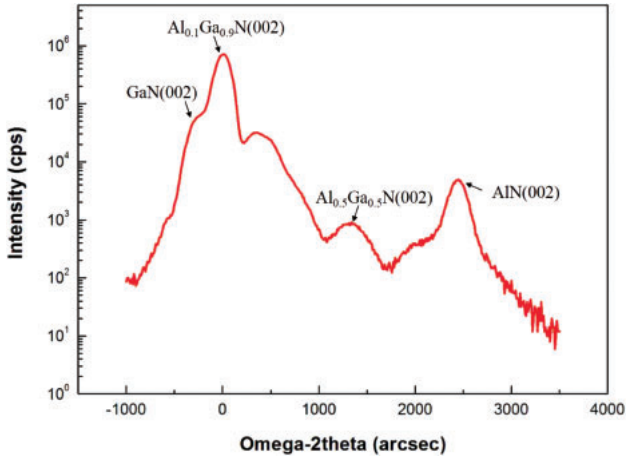

Fig. 4. XRD ω–2θ scan of the $Al_{0.2}Ga_{0.8}N/GaN/Al_{0.1}Ga_{0.9}N$ double heterostructure.

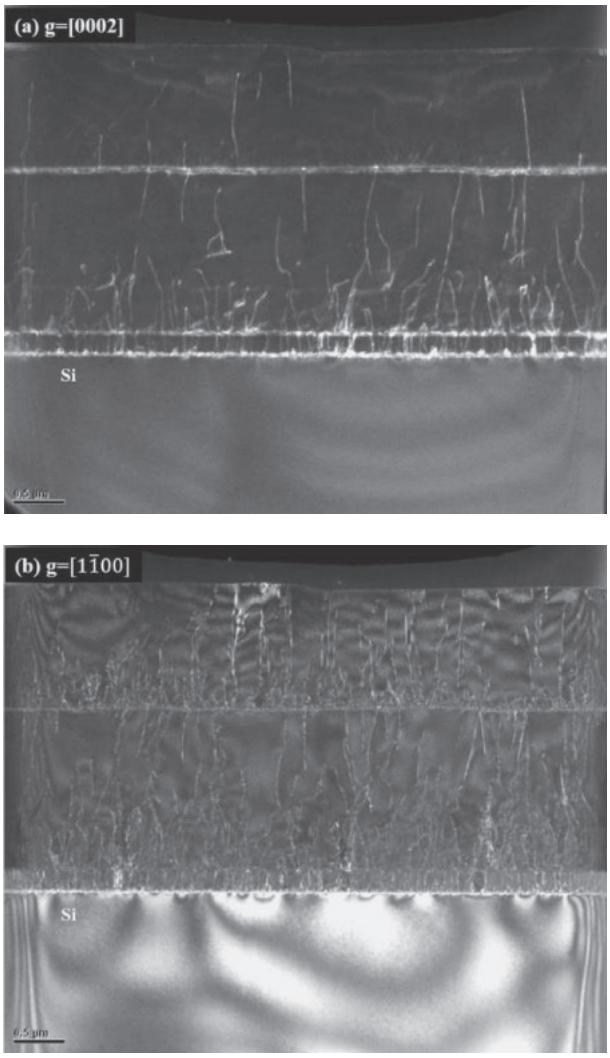

Fig. 5. Cross-sectional TEM images of whole epitaxial structure under weak-beam dark-field conditions of (a) $\mathbf{g} = [0002]$ and (b) $\mathbf{g} = [1\bar{1}00]$.

spectively. These results indicate that the crystalline quality of the $Al_{0.2}Ga_{0.8}N/GaN/Al_{0.1}Ga_{0.9}N$ double heterostructure on Si is comparable to that of the traditional AlGaN/GaN single heterostructure on Si.

The high crystalline quality of this interlayered structure was further confirmed from the cross-sectional TEM images of the heterostructure. The TEM images were taken to observe the dislocation distribution within the epilayers. Figure 5(a) shows the weak-beam dark-field TEM image under the $\mathbf{g} = [0002]$ condition. The edge dislocations with a Burgers vector of $\mathbf{b} = 1/3\langle 11\bar{2}0\rangle$ were invisible owing to the $\mathbf{g} \cdot \mathbf{b} = 0$ criterion. Only screw dislocations with a Burgers vector of $\mathbf{b} = \langle 0001\rangle$ and mixed dislocations with a Burgers vector of $\mathbf{b} = 1/3\langle 11\bar{2}3\rangle$ were observed. The number of screw dislocations in the upper $Al_{0.1}Ga_{0.9}N$ back barrier layer was significantly reduced after inserting the LT-AlGaN interlayer. The edge and mixed dislocations are shown in Fig. 5(b) under the $\mathbf{g} = [1\bar{1}00]$ condition. Here, the inserted LT-AlGaN interlayer shows less impact on the edge dislocation reduction. In order to enhance the breakdown voltage characteristics, it is necessary to grow a low-dislocation-density film. Hsu et al. and Dadgar et al. also indicated that the screw dislocations were the primary defects causing the decrease in the breakdown voltage.[20,21] Thus, the LT-AlGaN interlayer acts as a dislocation filter, which is very effective for screw dislocation reduction. This may explain the reason why the breakdown voltage was improved for the $Al_{0.1}Ga_{0.9}N$ back barrier with the LT-AlGaN interlayer.

Buffer leakage current measurement is a straightforward method of further evaluating the optimal structure design and material quality. The breakdown voltage of the epitaxial structure was determined by measuring the lateral buffer leakage characteristics across a 20 μm spacing. The buffer leakage currents of the three different epitaxial structures are shown in Fig. 6, which include the samples of (a) an $Al_{0.2}Ga_{0.8}N/GaN$ single heterostructure with a LT interlayer (total thickness: 3.4 μm), (b) an $Al_{0.2}Ga_{0.8}N/GaN/Al_{0.1}Ga_{0.9}N$ double heterostructure without a LT interlayer (total thickness: 2.3 μm), and (c) an $Al_{0.2}Ga_{0.8}N/GaN/Al_{0.1}Ga_{0.9}N$ double heterostructure with a LT interlayer (total thickness: 3.0 μm). The breakdown voltage characteristics of the samples from the first two conventional structures were below 400 V, but a breakdown voltage higher than 600 V was obtained from the sample of the $Al_{0.2}Ga_{0.8}N/GaN/Al_{0.1}Ga_{0.9}N$ double heterostructure with the LT interlayer. For the double heterostructure, the use of the $Al_{0.1}Ga_{0.9}N$ back barrier results in a lower

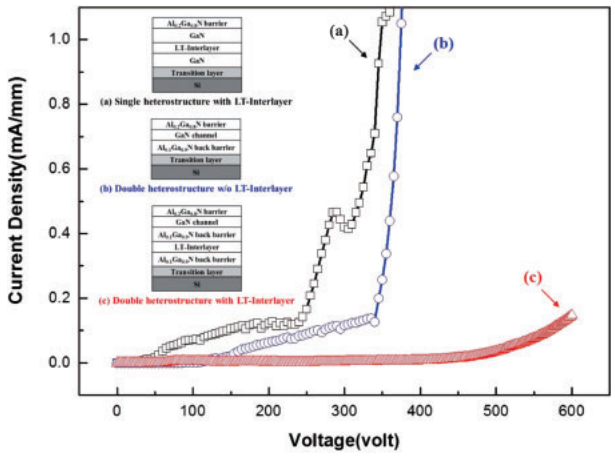

Fig. 6. Buffer leakage currents of various epitaxial structures.

buffer leakage current. Moreover, the thicker $Al_{0.1}Ga_{0.9}N$ back barrier with the improved crystalline quality also enhances the buffer breakdown voltage characteristics. On the basis of these advantages, an off-state breakdown voltage higher than 200 V was measured on the fabricated device using the proposed structure with a gate-to-drain spacing of 4.5 μm. This remarkable improvement demonstrates that the double heterostructure with the LT interlayer is an effective structure for high-power electronic applications.

In conclusion, an $Al_{0.2}Ga_{0.8}N/GaN/Al_{0.1}Ga_{0.9}N$ double heterostructure on Si with the inserted LT-AlGaN interlayer for breakdown voltage improvement is investigated. According to the SIMS depth profile, the interlayer can be regarded as the AlGaN interlayer. The thickness and Al composition of the LT-AlGaN interlayer as investigated by TEM and XRD are 21 nm and 50%, respectively. By in situ curvature measurement, the LT-AlGaN interlayer is observed to induce the compressive stress during the growth of the proposed structure. As shown in the weak-beam dark-field TEM analysis, the number of dislocations in the upper $Al_{0.1}Ga_{0.9}N$ back barrier is reduced by the insertion of the LT-AlGaN interlayer, especially for screw dislocations. Compared with the other conventional structures, the double heterostructure with the LT-AlGaN interlayer markedly improves the breakdown voltage of the device. The proposed structure with breakdown voltage higher than 600 V is demonstrated in this work. Overall, it is demonstrated that the proposed approach is very effective for increasing the buffer breakdown voltage of the double heterostructure and very promising for realizing devices for high-power applications.

Acknowledgments This work was sponsored by the NCTU-UCB I-RiCE program, Ministry of Science and Technology, Taiwan and TSMC under Grant No. NSC 103-2911-I-009-302, and the Ministry of Economic Affairs, Taiwan, under Grant No. 102-EC-17-A-05-S1-154.

1) J. Lee, B. Park, H. Lee, M. Lee, K. Seo, and H. Cha, Appl. Phys. Express **5**, 066502 (2012).
2) M. Sun, H. Lee, B. Lu, D. Piedra, and T. Palacios, Appl. Phys. Express **5**, 074202 (2012).
3) S. L. Selvaraj, A. Watanabe, A. Wakejima, and T. Egawa, IEEE Electron Device Lett. **33**, 1375 (2012).
4) J. J. Freedsman, T. Egawa, Y. Yamaoka, Y. Yano, A. Ubukata, T. Tabuchi, and K. Matsumoto, Appl. Phys. Express **7**, 041003 (2014).
5) P. Parikh, Y. Wu, and L. Shen, IEEE Energytech, 2013, p. 1.
6) B. J. Baliga, Semicond. Sci. Technol. **28**, 074011 (2013).
7) M. Su, C. Chen, and S. Rajan, Semicond. Sci. Technol. **28**, 074012 (2013).
8) S. L. Selvaraj, T. Suzue, and T. Egawa, IEEE Electron Device Lett. **30**, 587 (2009).
9) I. B. Rowena, S. L. Selvaraj, and T. Egawa, IEEE Electron Device Lett. **32**, 1534 (2011).
10) A. Dadgar, J. Bläsing, A. Diez, A. Alam, M. Heuken, and A. Krost, Jpn. J. Appl. Phys. **39**, L1183 (2000).
11) K.-W. Kim, D.-S. Kim, J.-H. Lee, and C.-K. Hahn, Electrochem. Solid-State Lett. **13**, H66 (2010).
12) S. Fritze, P. Drechsel, P. Stauss, P. Rode, T. Markurt, T. Schulz, M. Albrecht, J. Bläsing, A. Dadgar, and A. Krost, J. Appl. Phys. **111**, 124505 (2012).
13) J. Bläsing, A. Reiher, A. Dadgar, A. Diez, and A. Krost, Appl. Phys. Lett. **81**, 2722 (2002).
14) A. Reiher, J. Bläsing, A. Dadgar, A. Diez, and A. Krost, J. Cryst. Growth **248**, 563 (2003).
15) G. Cong, Y. Lu, W. Peng, X. Liu, X. Wang, and Z. Wang, J. Cryst. Growth **276**, 381 (2005).
16) W. Liu, J. J. Zhu, D. S. Jiang, H. Yang, and J. F. Wang, Appl. Phys. Lett. **90**, 011914 (2007).
17) E. Frayssinet, Y. Cordier, H. P. D. Schenk, and A. Bavard, Phys. Status Solidi C **8**, 1479 (2011).
18) K. Cheng, H. Liang, M. Van Hove, K. Geens, B. De Jaeger, P. Srivastava, X. Kang, P. Favia, H. Bender, S. Decoutere, J. Dekoster, J. del Agua Borniquel, S. W. Jun, and H. Chung, Appl. Phys. Express **5**, 011002 (2012).
19) Y.-L. Hsiao, C.-A. Chang, E. Y. Chang, J. S. Maa, C.-T. Chang, Y.-J. Wang, and Y.-C. Weng, Appl. Phys. Express **7**, 055501 (2014).
20) J. W. P. Hsu, M. J. Manfra, R. J. Molnar, B. Heying, and J. S. Speck, Appl. Phys. Lett. **81**, 79 (2002).
21) A. Dadgar, T. Hempel, J. Bläsing, O. Schulz, S. Fritze, J. Christen, and A. Krost, Phys. Status Solidi C **8**, 1503 (2011).